

We are IntechOpen, the world's leading publisher of Open Access books Built by scientists, for scientists

6,900

Open access books available

186,000

International authors and editors

200M

Downloads

Our authors are among the

154

Countries delivered to

TOP 1%

most cited scientists

12.2%

Contributors from top 500 universities



WEB OF SCIENCE™

Selection of our books indexed in the Book Citation Index
in Web of Science™ Core Collection (BKCI)

Interested in publishing with us?
Contact book.department@intechopen.com

Numbers displayed above are based on latest data collected.
For more information visit www.intechopen.com



Efficient Computer-Aided Techniques to Detect Glaucoma

Nataraj Vijapur and R. Srinivasarao Kunte

Abstract

A survey of the World Health Organization has revealed that retinal eye disease Glaucoma is the second leading cause for blindness worldwide. It is a disease which will steal the vision of the patient without any warning or symptoms. About half of the World Glaucoma Patients are estimated to be in Asia. Hence, for social and economic reasons, Glaucoma detection is necessary in preventing blindness and reducing the cost of surgical treatment of the disease. The objective of the chapter is to predict and detect Glaucoma efficiently using image processing techniques. We have developed an efficient computer-aided Glaucoma detection system to classify a fundus image as either normal or glaucomatous image based on the structural features of the fundus image such as cup-to-disc ratio (CDR), rim-to-disc ratio (RDR), superior and inferior neuroretinal rim thicknesses, vessel structure-based features, and distribution of texture features in the fundus images. An automated clinical support system is developed to assist the ophthalmologists to identify the persons who are at risk in the early stages of the disease, monitor the progression of the disease, and minimize the examination time.

Keywords: glaucoma, cup-to-disc ratio (CDR), rim-to-disc ratio (RDR), superior, inferior, neuroretinal rim, structure features, texture features

1. Introduction

According to the survey of the World Health Organization, over the last 10 years, cataract remains the highest leading cause of blindness worldwide covering 47.9% of overall blindness. It is a progressive and painless clouding of the internal lens of the eye. Similarly, the survey declares Glaucoma as the second leading cause for blindness worldwide. About 12.3% of patients in the world are suffering from Glaucoma [1]. It is a disease which will steal the vision of the patient without any warning or symptoms. Surveys conducted in North America and Europe revealed a significant proportion of new Glaucoma patients who were previously gone undetected. The proportion estimated for Glaucoma patients in Asia and developing countries is even larger [2]. This calls for the need for early Glaucoma detection, and we can prevent blindness and reduce the surgical cost involved in treating the disease. The fundus image of the eye, Glaucoma disease, structural changes in fundus image due to Glaucoma, and its diagnosis are presented in this section.

1.1 Fundus image of the eyes

The eye is the most complex organ of the human body with approximate dimension of 2.54 cm width, 2.3 cm height, and 2.54 cm deep [3]. The human eye acts like a camera [4] and processes the visual signals. **Figure 1** shows the front view of the eye fundus image consisting of the optic disc and optic cup. The optic nerves and blood vessels exit the retina from the optic disc. It is considered as one of the main features of a retinal fundus image and is located to the nasal side of the fovea. It is vertically oval, with an average dimension of horizontally 1.76 mm and vertically 1.92 mm. Inside the optic disc, there is a central depression, of variable size, called the optic cup.

The optic nerve head is the location where ganglion cell axons exit the eye to form the optic nerve. The changes in the shape and color or depth of the optic disc and optic cup are the indicators of various ophthalmic pathologies especially for Glaucoma and other eye diseases. Optic disc and cup are the brightest features of the normal fundus. The disc appears to be as a bright yellow or white region in colored fundus image.

1.2 Structural changes in fundus image due to glaucoma

The structure and appearance of the optic disc can reveal the presence of Glaucoma, and they are considered as very important features to assess the damage due to Glaucoma. The optic cup concentric enlargement, decrease in rim area, and other such patterns of glaucomatous damage are most commonly found. The ratio of area of optic cup to area of the optic disc is normally considered to evaluate the disease. Due to Glaucoma, in the retina the optic cup area enlarges and progresses toward the disc. This distinction can be seen between normal and Glaucoma-affected fundus images as shown in **Figure 2(a)** and **(b)**, respectively. This cup-to-disc area ratio (CDR) is used in ophthalmology to determine the progression of Glaucoma. If the CDR value is greater than 0.3, the patient has a threat of Glaucoma. The CDR of the image in **Figure 2(b)** is nearly 0.7, and it is a prominent case of Glaucoma.

The area present between the cup and disc boundary of the eye is termed as neuroretinal rim [5] as shown in **Figure 3(a)** and **(b)** for a sample of normal and Glaucoma eye, respectively. Thinning of the neuroretinal rim is also one of the symptoms of Glaucoma. Rim-to-disc area ratio (RDR) is also an indicator

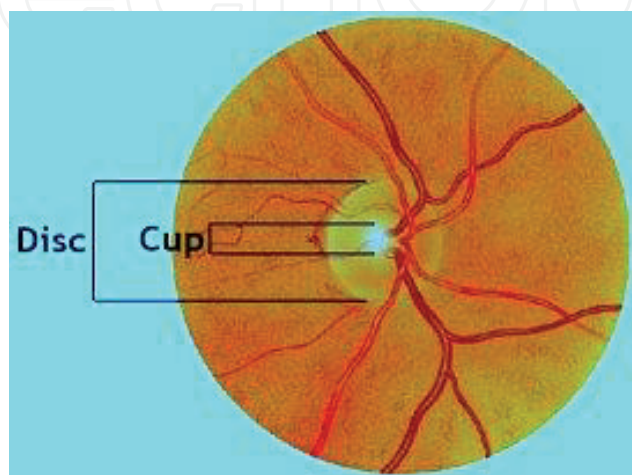


Figure 1.
Front view of the eye fundus image.

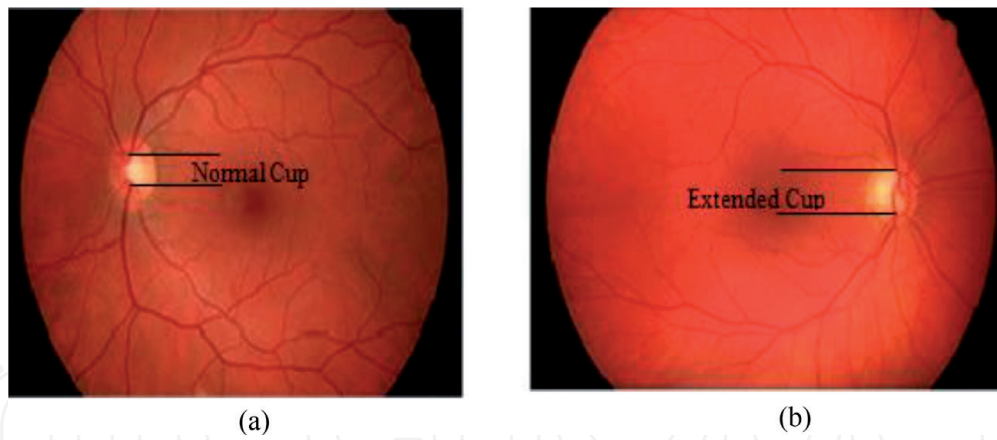


Figure 2.
Fundus images: (a) normal eye; (b) glaucoma eye.

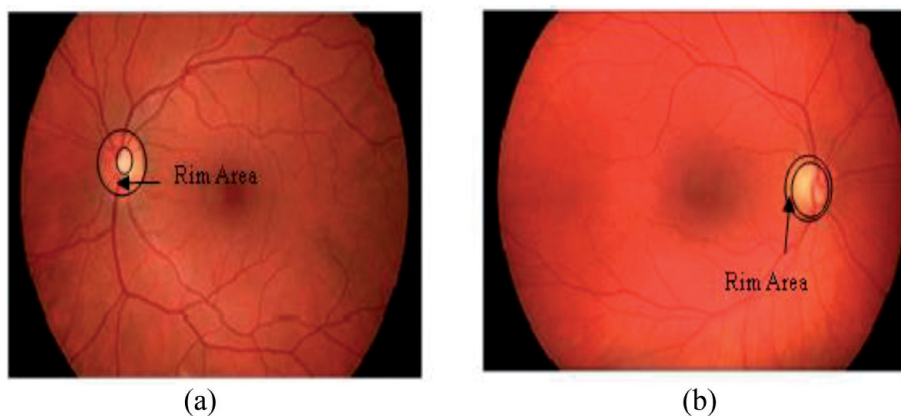


Figure 3.
Neuroretinal rim: (a) rim area in the normal eye; (b) rim area in the Glaucoma eye.

for Glaucoma. As seen from **Figure 3**, the normal eye has more RDR than the Glaucoma eye.

The retinal image shall be seen as composed of inferior, superior, nasal, and temporal regions as shown in **Figure 4(a)**. Due to Glaucoma, blood vessels covered by the nasal region increase, and the inferior–superior region decreases. Hence, the ratio of the area of the sum of blood vessels in the inferior–superior region to the sum of blood vessels in the nasal-temporal region (ISNT) decreases. This feature can also be used to detect Glaucoma more accurately [5, 6].

A study has revealed that the diameters of the retinal vessels have been seen to be significantly smaller in the glaucomatous eyes than the normal eyes [7, 8]. This reduction in vessel diameters can be continuously monitored, and the disease can be detected in early stages. Also, in the case of prominent cases of Glaucoma, there is a distortion observed in cup structure. Cup usually expands downward more toward inferior side. Therefore, disease can be detected by measuring the difference in neuroretinal rim thickness at the superior and inferior regions, which are referred as superior rim thickness and inferior rim thickness as shown in **Figure 4(b)**.

In the case of Glaucoma, thickness of the vessels around the disc goes on reducing due to lack of fresh aqueous humor. This also results in disappearance of small vessels around the disc. A normal eye contains a lot of very minute vessels like small branches of tree around the optic disc, which are absent in the Glaucoma eye as shown in **Figure 5**.

In the normal eye, peripheral vision is present fully. In the Glaucoma-affected eye, peripheral vision goes on reducing. As an illustration, **Figure 6(a)** shows the

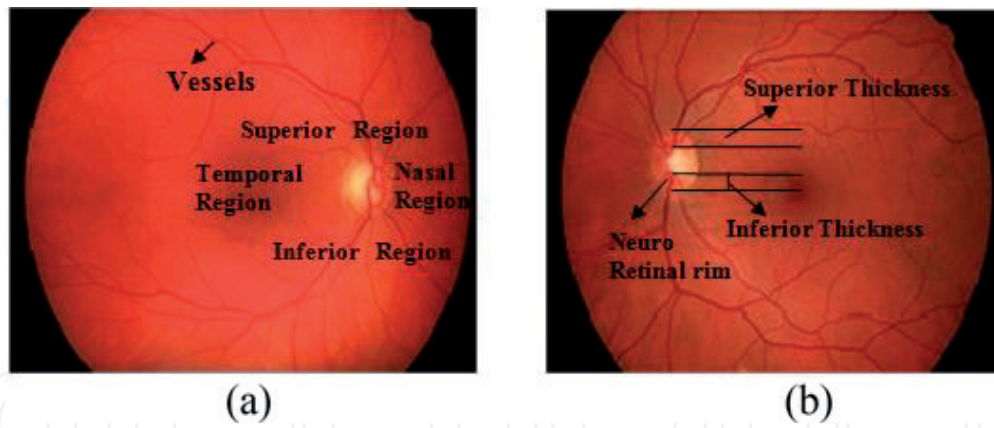


Figure 4. Regions of fundus image: (a) ISNT regions and vessels, (b) neuroretinal rim and superior and inferior thicknesses.

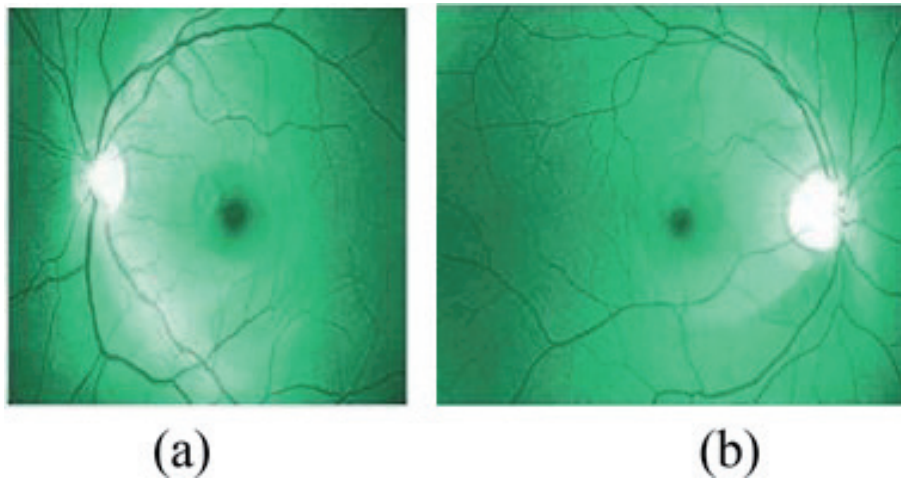


Figure 5. Vessels in fundus image: (a) a normal eye as seen through the green filter; (b) a glaucoma eye in green filter.



Figure 6. Vision loss due to Glaucoma: (a) normal eye vision; (b) glaucoma eye vision (courtesy: <http://www.caeps.org/>).

vision of a sample picture as perceived by a normal eye, and **Figure 6(b)** shows the vision of the same picture as perceived by a Glaucoma eye.

1.3 Fundus features used for glaucoma detection

We have used the fundus features such as (i) CDR, (ii) RDR, (iii) superior rim thickness, (iv) inferior rim thickness, (v) structural features of vessels around

the disc such as maximum vessel diameter, number of vessel segments, and total number of smaller diameters of vessels, and (vi) spatial textures to detect Glaucoma by the digital image processing techniques [9–12].

2. Proposed comprehensive efficient integrated glaucoma detection system

The block schematic of our proposed comprehensive efficient integrated Glaucoma detection system for Glaucoma identification using image processing techniques is shown in **Figure 7**.

The retinal image of the eye is captured using a fundus camera. The captured eye fundus image is subjected to various image processing techniques to extract different features of fundus image.

Our proposed system extracts and uses the following three different sets of fundus eye image features for detection of Glaucoma:

Fundus structure based features (CDR, RDR and Neuroretinal rim thicknesses), Vessel structural features and Textural features.

Structure-based features of fundus image are extracted using a template-based approach. A template aids the segmentation of the optic cup and disc from the fundus image. A template is correlated with fundus image using Pearson-r correlation for segmentation. Structure-based features such as CDR, RDR, and superior and inferior rim thicknesses are extracted.

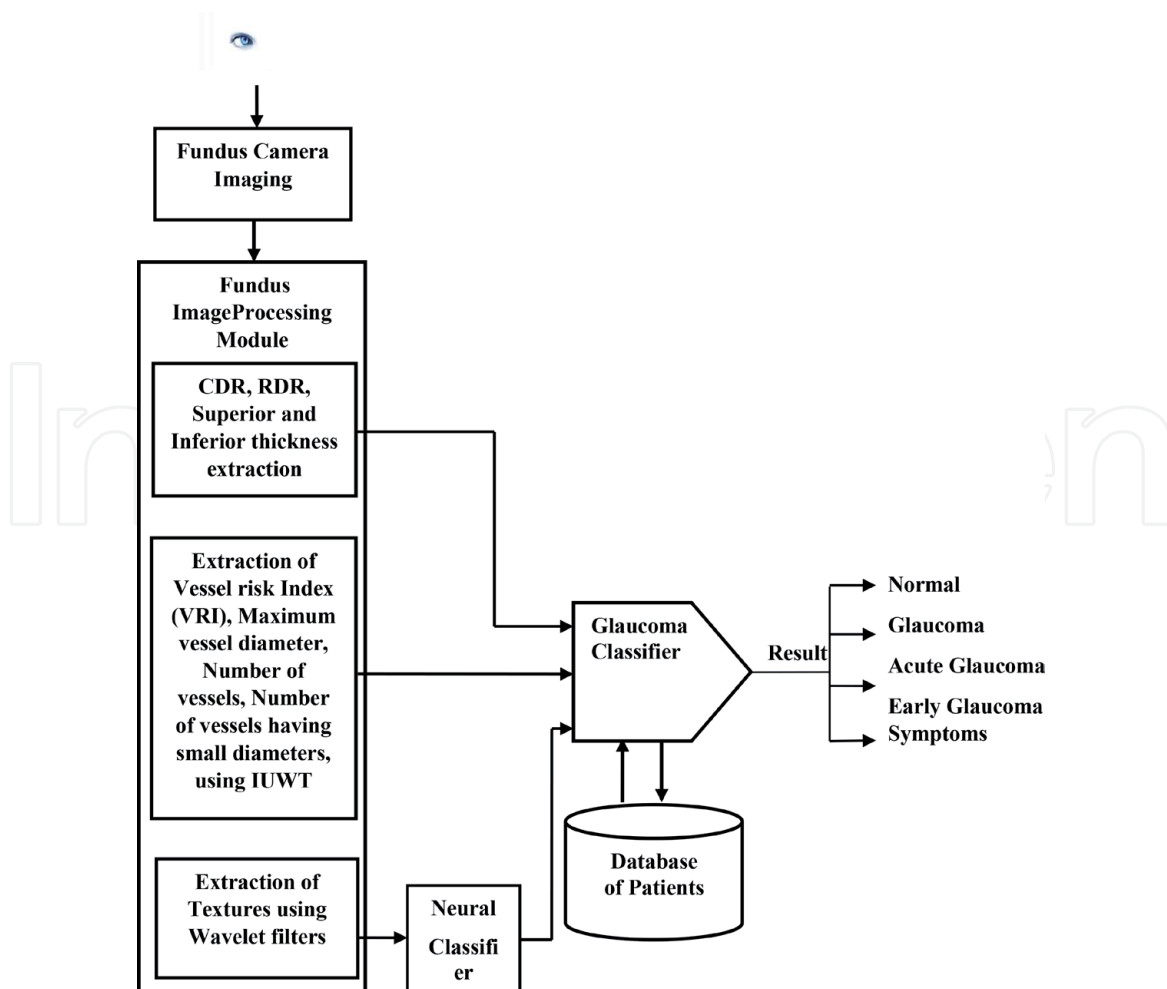


Figure 7.
Comprehensive efficient integrated glaucoma detection system.

Fundus images' vessel structure-based features such as vessel count, vessel diameters, maximum vessel diameter, and count of vessels having fewer diameters are extracted using isotropic undecimated wavelet transform (IUWT).

Fundus images' texture features are extracted using three families of wavelet filters: daubechies (db3), symlets (sym3), and biorthogonal (bio3.3, bio3.5, and bio3.7) wavelet filters. A trained neural classifier fed with the texture features classifies the given test image into a normal or Glaucoma image as the first stage of classification.

Based on the literature survey and suggestion of ophthalmologists, the ultimate Glaucoma classifier is developed. The above set of extracted features and neural classifier output are fed to the final classifier. It finally classifies the given test image as either (i) normal or (ii) Glaucoma or (iii) acute Glaucoma or (iii) early Glaucoma symptom image.

The extracted features like CDR, RDR, superior and inferior rim thicknesses, vessel count, vessel diameter, maximum vessel diameter, and count of vessels having fewer diameters are stored in a database meant for the patient. These features can be used to assess the progression of the disease during the next visit of the patient. This will assist the ophthalmologists for better monitoring of patients. Database will be very useful for mass screening programs and also plays an important role in detecting Glaucoma at an early stage in the case of risk patients who are having genetic background of Glaucoma.

2.1 Sources of image dataset used for the development of proposed glaucoma detection system

For our Glaucoma detection system experiments, analysis, and testing results, we have used the glaucomatous fundus image dataset and normal image dataset from the following sources:

High-Resolution Fundus (HRF) image dataset, available on the public domain <https://www5.cs.fau.de/research/data/fundus-images/>. This dataset has been established by a collaborative research group to support research and comparative studies on retinal fundus images [13, 14], which is used by many researchers for their experiments and testing results. This dataset comprises of a set of 15 Glaucoma and 15 normal images and fundus images available at KLE Dr. Prabhakar Kore Hospital, Belagavi, India, which have been captured using a Canon CF1 High-Resolution fundus camera with a 50° field of view. Each image was captured using 24 bits per color plane at dimensions of 2534 × 2301 pixels.

We are referring the above two datasets in our thesis as (i) HRF dataset and (ii) Hospital dataset, respectively.

2.2 Glaucoma detection using template

This chapter presents an efficient methodology developed for the automatic localization and segmentation of the optic cup and disc in retinal images followed by extraction of some structural features for Glaucoma detection. Localization of the optic disc in the retinal image and extraction of the features are done by correlating the fundus image with a newly developed template using Pearson-r correlation. Segmentation of the optic cup and disc is done on the basis of correlation levels [15–18].

2.2.1 Preprocessing

Our proposed methodology is based on correlating the fundus image with a designed template. The template is designed based on intensity distribution of the

fundus image. Hence, it is required to determine the intensity component of the input image. The true color format of the fundus image captured by the fundus camera does not reveal the intensity component value directly, whereas hue, saturation, and intensity (HSI) format representation of an image directly provide the intensity component value of an image (refer to **Figure 8**). Therefore, the RGB format captured by the fundus image is converted into HSI format in the pre-processing stage.

Conversion from RGB to HSI is achieved using the following equations:

$$I(\text{intensity}) = \frac{R(\text{red}) + G(\text{green}) + B(\text{blue})}{3} \quad (1)$$

$$H(\text{hue}) = \cos^{-1} \left\{ \frac{\frac{1}{2}[(R - G) + (R - B)]}{[(R - G)^2 + (R - B)(G - B)]^{\frac{1}{2}}} \right\} \quad (2)$$

$$S(\text{saturation}) = 1 - \frac{3}{(R + G + B)}[\min(R, G, B)] \quad (3)$$

A sample RGB fundus image and its corresponding converted HSI image is shown in **Figure 8**.

2.2.2 Glaucoma detection using Pearson-r coefficient extraction

Further, the intensity component of the fundus image is correlated with a template designed using Pearson-r correlation to localize the optic disc in the image. The template is designed keeping in view the general structure of the optic disc and cup. The size of the optic disc varies significantly with the different fundus images. We observed that the optic disc widths varied from 60 to 100 pixels in the images of our dataset. The optic disc consists of a rim and cup. The intensity of the rim is higher than the rest of the image outside the rim, and the cup is the brightest part of the fundus image. We have designed a square-shaped image template to have a disc with a rim and cup as shown in **Figure 9(a)**. The cup will have the highest intensity, and intensity decreases toward the rim and other outer parts of the image similar to intensity distribution pattern of a fundus image. A Laplacian of Gaussian distribution is used to get this intensity distribution pattern. Pearson-r coefficients are extracted from correlating the template with the preprocessed image. The correlated image contains the information of optic cup and disc in the form of intensity variation with respect to template image from the fundus image. As seen from **Figure 8(b)** for a sample correlated image, the optic disc and cup can be very easily separated on an intensity plane.

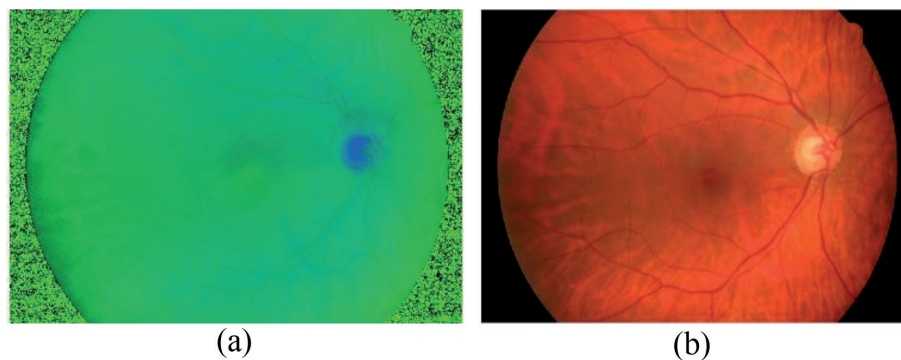


Figure 8.
 Preprocessing stage: (a) input fundus RGB image; (b) converted HSI image.

Further, the optic cup and disc are easily segmented as they differ in their correlated magnitudes. Binary images of the segmented optic disc, cup, and rim are shown in **Figure 10**.

Figures 11 and **12** show the segmentation of optic cup and disc and neuroretinal rim in binary image for a sample image of Hospital dataset and HRF dataset, respectively.

The values of CDR, RDR, and superior and inferior rim thicknesses are calculated from the extracted image.

2.3 Glaucoma detection using vessel segmentation

According to the literature survey due to progression of Glaucoma, blood vessel diameter decreases [19–22], and smaller diameter vessels around the optic disc start diminishing and disappearing. We have employed these aspects of vessels as features to detect the Glaucoma at an early stage. **Figure 13** clearly shows these aspects. The region where these significant vessels of interest are present in a small area around the optic disc in the image for detection of Glaucoma is considered as region of interest (ROI).

2.3.1 ROI extraction

In previous section, we presented the methodology of segmenting the optic disc by correlating the input fundus image with designed template using Pearson-r

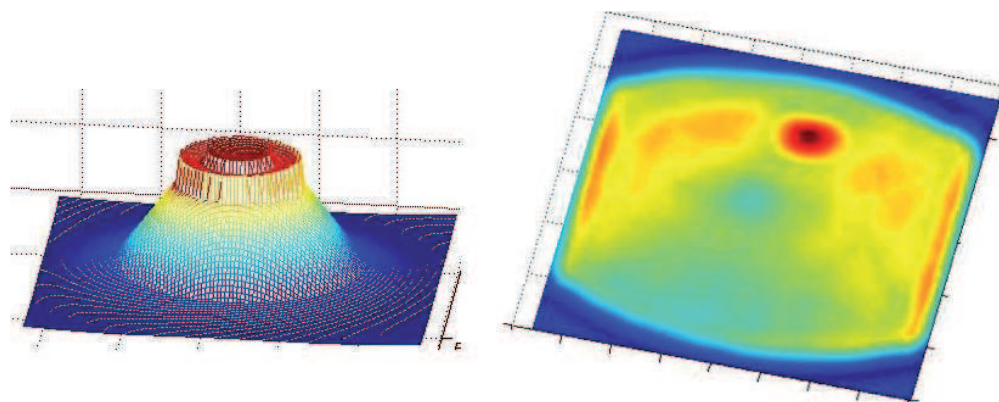


Figure 9. Correlation: (a) correlation filter; (b) intensity distribution of correlated fundus.

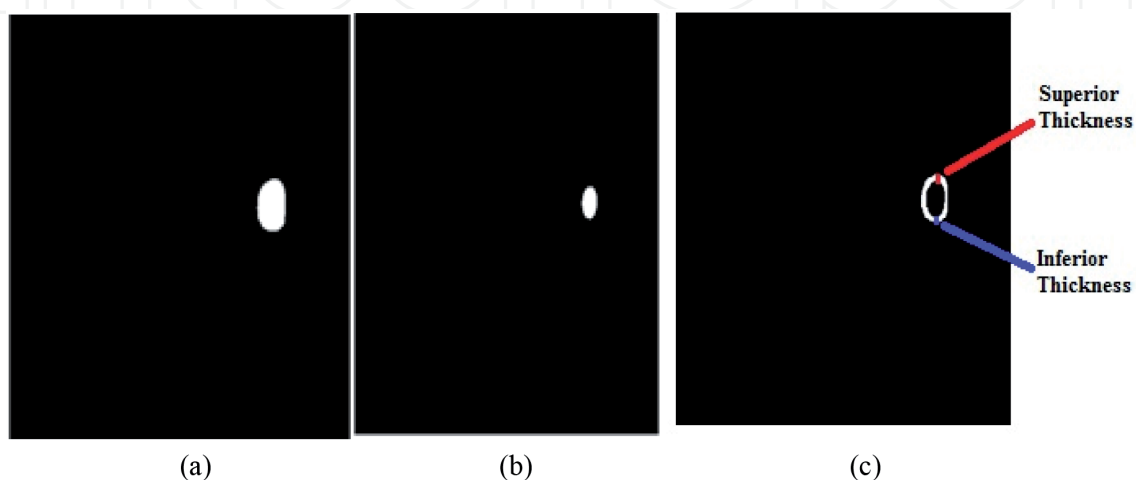


Figure 10. Segmentation. (a) Segmented optic disc. (b) Segmented optic cup. (c) Neuroretinal rim thickness.

correlation. The value of Pearson-r correlation is maximum at the center of the optic disc which corresponds to the brightest spot in the fundus image. After segmenting the disc as discussed in Section 2.2.2, its boundary points on the top,

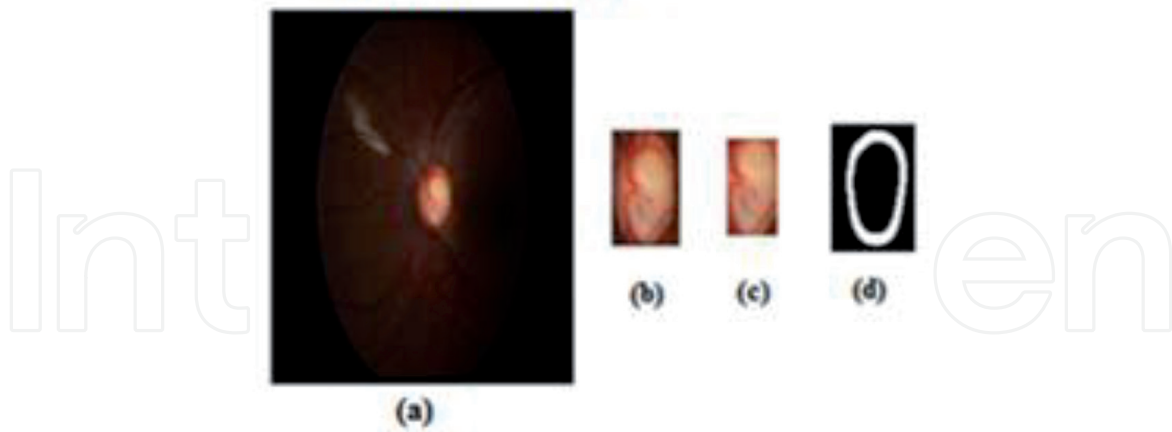


Figure 11.
Hospital dataset sample. (a) Original sample. (b) Segmented optic disc. (c) Segmented optic cup. (d) Binary image showing neuroretinal rim.

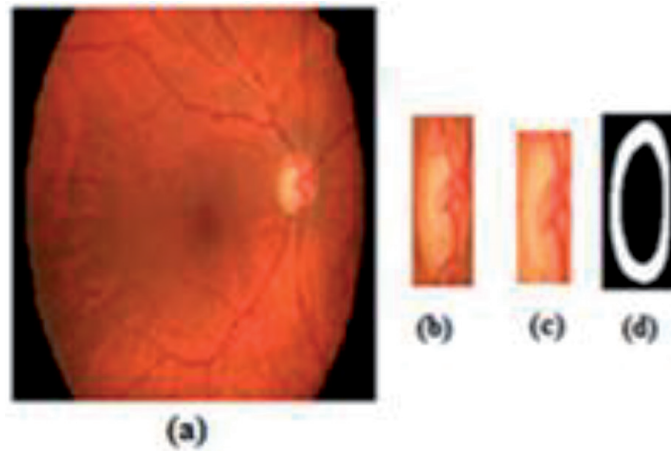


Figure 12.
HRF dataset sample. (a) Original sample. (b) Segmented optic disc. (c) Segmented optic cup. (d) Binary image showing neuroretinal rim.

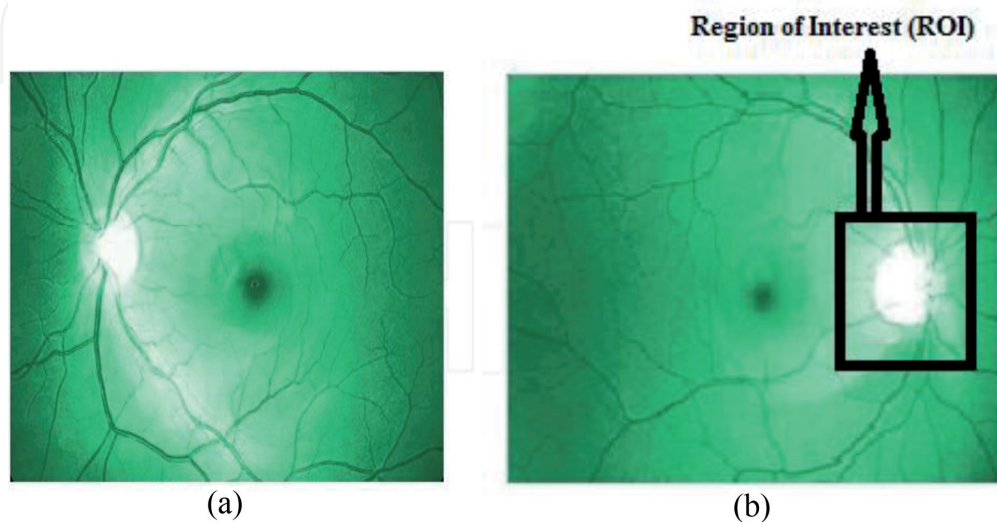


Figure 13.
Vessels in fundus image showing ROI: (a) vessels in the normal eye with smaller vessels around the optic disc; (b) the absence of smaller vessels around the optic disc in the glaucoma eye.

bottom, left, and right sides are identified, thus localizing it. A sample fundus image from our dataset and its corresponding identified ROI image part are shown in **Figure 14**.

In signal processing applications, analysis of signal in frequency domain is preferred over the time domain since they contain more information of the signal. This requires conversion of the signal from time domain to frequency domain. Fourier transform can be used to obtain the frequency contents of a signal. But it does not reveal which frequency component is present at what time instance of the signal. Wavelet transform, on the other hand, reveals this information and conveys more detailed information regarding the signal or the image. In image processing techniques such as segmentation, image decomposition using undecimated biorthogonal wavelet transforms is employed, as these transforms also facilitate reconstruction of the images [23]. For segmentation of astronomical and biological images where images contain isotropic objects, the isotropic undecimated wavelet transform (IUWT) can be applied for segmentation. In the fundus images, vessels are isotropic in nature. Hence IUWT can be used for segmentation of vessels. When ROI is subjected to IUWT, decompositions at different wavelet levels are shown in **Figure 15**.

2.3.2 Vessel localization

For further processing, an image with a wavelet level of 3 is considered. To obtain the centerline of each of the segmented vessels, they are subjected to a thinning process which converts a vessel into a thin vessel of one pixel thickness. The position of this thin vessel will be almost in the center of the vessel, and it represents the centerline of the vessel. A sample of segmented vessels of ROI is shown in **Figure 16(a)**. The output of the thinning process of the sample vessels is shown in **Figure 16(b)**, which depicts the thinned centerlines of vessels. **Figure 16(c)** depicts the identified thinned branches after removing the branch pixels. Each thin line in the image of **Figure 16(c)** represents a separate vessel. Now, each thin line in the image represents a separate vessel.

Using connected component technique, each line (vessel) in the image is indexed and can be accessed with that index. Further, using the index information, the coordinates of the centerline pixels of each vessel are determined, thereby localizing the vessels. Further, the vessel data structure is created and maintained

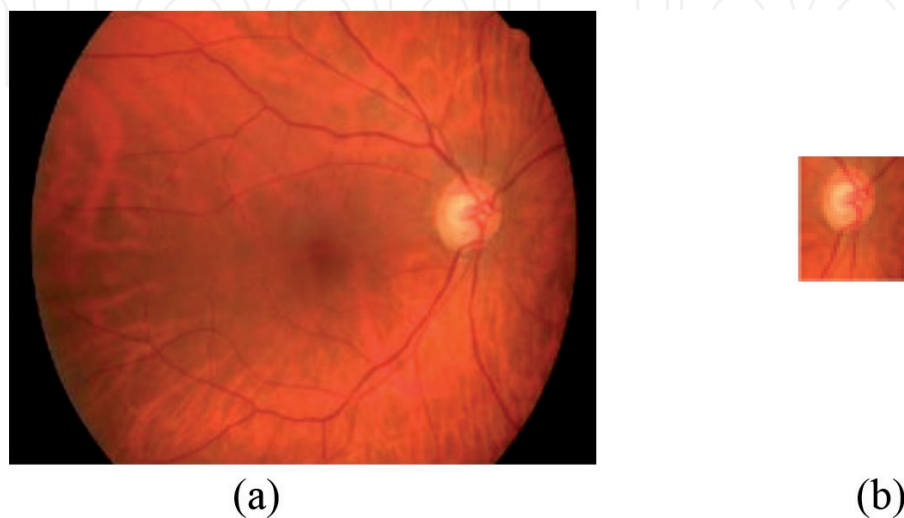


Figure 14.
(a) Input image. (b) Extracted ROI.

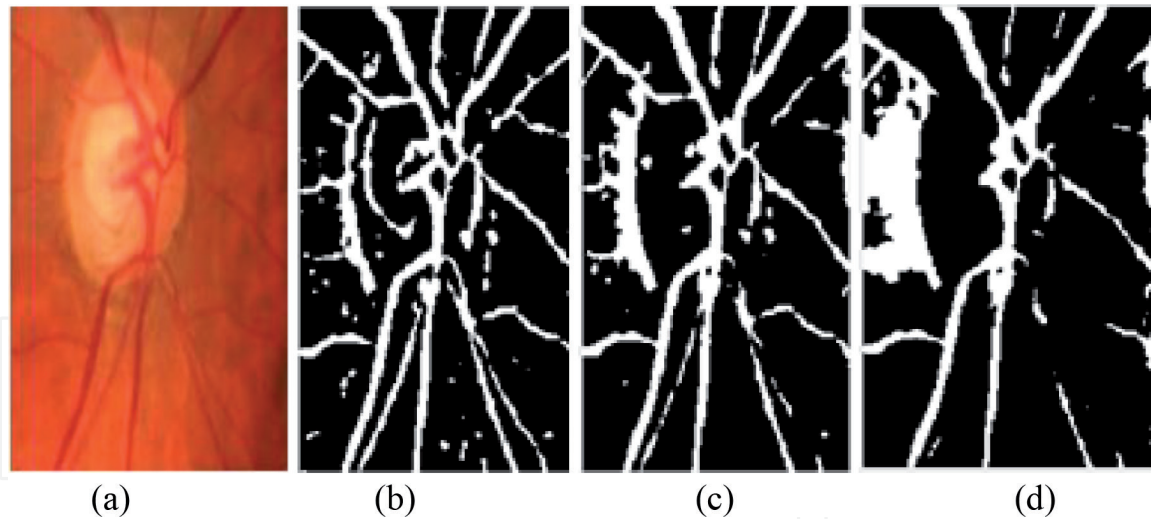


Figure 15.
(a) Extracted ROI. (b) Image with low wavelet level of 3. (c) Image with high wavelet level of 4. (d) Image with wavelet level of 5.

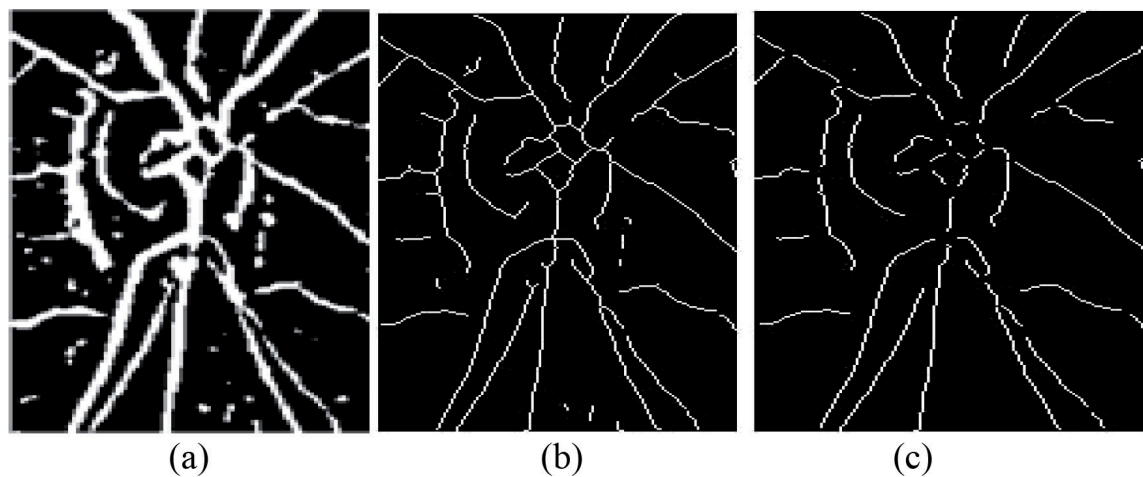


Figure 16.
(a) Vessels from the segmented image. (b) Thinned centerlines and (c) centerlines with branches separated.

which contains the entire information regarding the vessels. Vessel-based feature vessel risk index (VRI) is extracted from the information obtained in vessel data structure [18].

2.4 Glaucoma detection methodology using wavelet texture features

The block diagram of the methodology used is shown in **Figure 17**. The input fundus image is preprocessed for removal of background noise. Preprocessed image is decomposed by using wavelet filters to obtain the approximation and detail coefficients of the image. From these coefficients, texture features are generated. These texture features are fed to the ANN classifier to detect Glaucoma. In the preprocessing stage, arithmetic mean filter [20] is used to remove the background noise of the fundus image.

2.4.1 Image decomposition and texture feature extraction

The preprocessed image is decomposed by applying the wavelets. The set of 14 wavelet features' average and energy values are considered as the texture

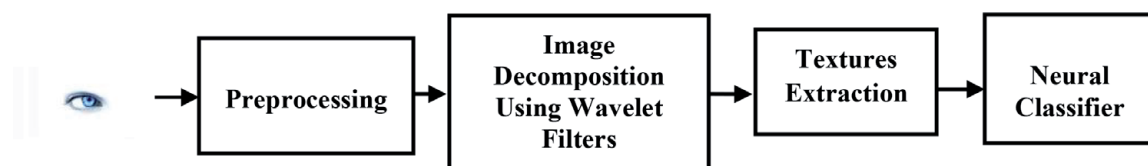


Figure 17.
Block schematic of glaucoma detection using texture features.

features of an image which can be used for classification of the image as normal or Glaucoma image.

We apply the three wavelets daubechies (db3), symlets (sym3), and biorthogonal (bio3.3, bio3.5, and bio3.7) separately for the fundus image and first obtain the approximation and the detail coefficients. Later, we compute the average and the energy values from these coefficients.

Among the average and energy values, we have used only average value of the horizontal information and energy of vertical information for all the wavelets (db3, sym3, bio3.3, bio3.5, and bio3.7). In addition, we have used the diagonal energy values for bio3.3, bio3.5, and bio3.7 and horizontal energy value for bio3.7, totaling to 14 texture values all together from all the wavelets. The other average and energy values are not used since their values for the normal and Glaucoma images lie in the same range, which has been verified by analyzing the values. This selection also has been reported in [24]. The texture values extracted from a fundus image are fed to the neural classifier for classification.

2.4.2 Neural classifier

Classification using ANN is the state-of-the-art technique employed for efficient classifications. We have used feedforward ANN with modified backpropagation training technique to implement the classifier. Feedforward multiple layer perceptron (MLP) neural networks are one of the important types of neural networks. They are widely used in recognition systems due to their good generalization property. MLPs consist of multiple layers as shown in **Figure 18**. It has one input and one output layer. One or more hidden layers are used in between input and output layers. The number of neurons in the input layer depends on the number of inputs to be fed to the network, and the number of neurons in the output layer depends on the number of outputs to be generated for the final classifier output. Hidden layers can have any number of neurons. Output of a neuron of input/hidden layer is connected to the input of all neurons in the next layer in fully connected network, as shown in **Figure 19**.

2.4.3 Glaucoma neural classifier architecture

We used a 4-layer MLP with input layer, two hidden layers, and output layer. For each input fundus image, 14 wavelet features are extracted. To feed these 14 features, input layer has 14 neurons. As the output result we want it to be either normal or Glaucoma indication, the output layer consists of only one neuron. We used two hidden layers with 14 neurons in each layer as we could get better results with two hidden layers than one. The architecture of the neural classifier used is shown in **Figure 18**.

Different training methods can be used to train the MLPs for classification. We employed the modified popular backpropagation training algorithm with the minimum

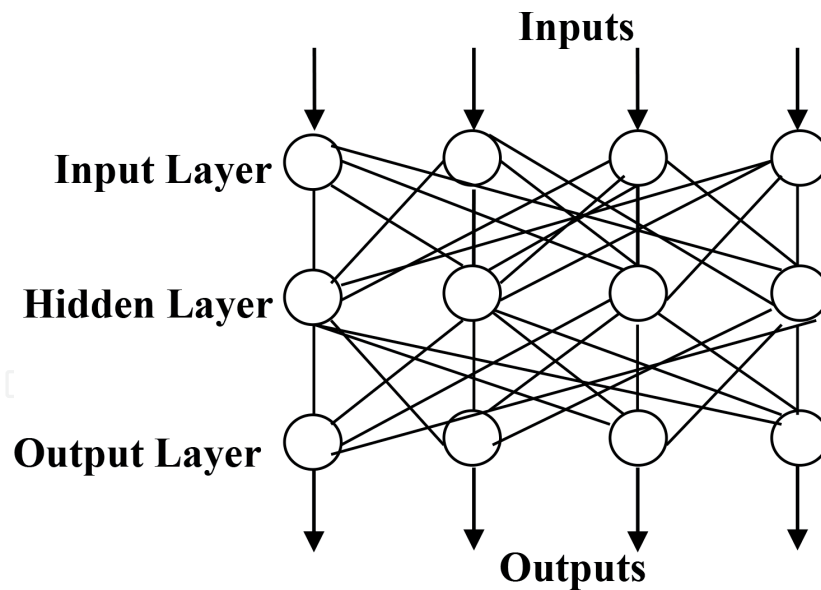


Figure 18.
 Architecture of glaucoma neural classifier.

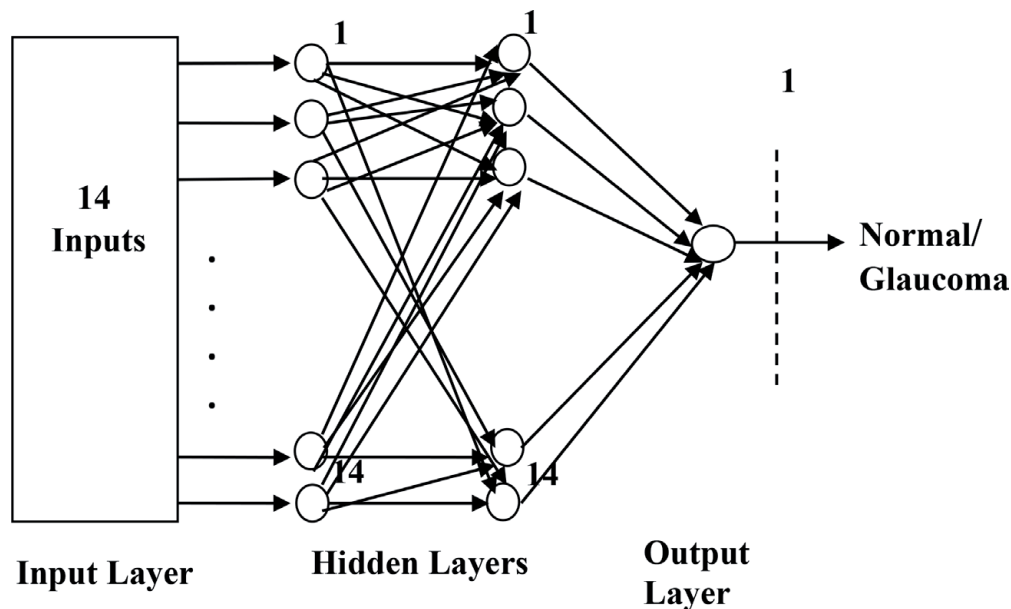


Figure 19.
 Feedforward neural network.

mean square error performance as a function for training our neural classifier. Levenberg–Marquardt method [25, 26] of optimization is used to train the classifier.

3. Results and discussion

Our final proposed integrated Glaucoma classifier system considers all these proposed features for classification. The structural features are related to the optic disc and cup such as CDR, RDR, and superior and inferior rim thicknesses, which are extracted using template methodology. VRI, the vessel structural feature, and texture features are obtained by wavelet filters. This aspect of incorporating more features has led to improvement of the efficiency of Glaucoma detection which can be seen from comparison of results as shown in **Table 1**. Totally, 120 Glaucoma images and 60 normal images were used from the datasets for comparison.

Image type	Results of using vessel-based feature VRI	Results of feature extraction using NSK template	Results of using wavelets and neural classifier	Results of final integrated glaucoma classifier
Glaucoma dataset	85%	94%	95%	98.57%
Normal dataset	83%	90%	94%	94%

Table 1.
Results of glaucoma classifier.

4. Conclusions

Literature survey reveals that previous attempts were made to detect Glaucoma by extracting predominantly CDR or wavelet-based features. In our research work of Glaucoma detection, we have enhanced the efficiency of Glaucoma detection system by processing and analyzing additional fundus image features apart from the CDR or wavelet features leading to a hybrid approach.

We have also improved the efficiency of CDR-based Glaucoma detection system by a template for correlation with input fundus images. As seen from Results section, template correlation approach is better than intensity threshold techniques. Additional features, RDR and neuroretinal rim thickness, have improved the efficiency of the system.

We have introduced vessel-based features for Glaucoma detection which is a significant step toward Glaucoma detection. As seen in the literature, reductions in vessel diameters are the indication of Glaucoma. To detect this we have incorporated database where these significant features can be stored and monitored for regular visits of patients.

Wavelet-based strategy has also been used by us to increase the efficiency of the system. We have used feedforward neural networks to classify the input fundus images using wavelet-based textures.

Acknowledgements

We would like to express our sincere gratitude to Ophthalmology department of KLE Society's Dr. Prabhakar Kore Hospital & M.R.C., Belagavi, India, for providing us with necessary guidance and resources required for experimentation and special thanks to High-Resolution Fundus (HRF) Image Database available on the Internet [13]. We would like to thank Research Center, E & C Department of Jawaharlal Nehru National College of Engineering, Shivamogga, India, and Electronics and Communication Department, KLE Dr. M.S. Sheshgiri College of Engineering and Technology, Belagavi, India, for technical guidance and resources, without which venture would not have been possible.

IntechOpen

Author details

Nataraj Vijapur^{1*} and R. Srinivasarao Kunte²

1 KLE Dr. M.S. Sheshgiri College of Engineering and Technology, Belagavi, Karnataka, India

2 Sahyadri College of Engineering and Management, Mangalore, Karnataka, India

*Address all correspondence to: nvijapur@gmail.com

IntechOpen

© 2020 The Author(s). Licensee IntechOpen. This chapter is distributed under the terms of the Creative Commons Attribution License (<http://creativecommons.org/licenses/by/3.0>), which permits unrestricted use, distribution, and reproduction in any medium, provided the original work is properly cited. 

References

- [1] Raychaudhuri A, Lahiri SK, Bandyopadhyay M, Foster PJ, Reeves BC, Johnson GJ. A population based survey of the prevalence and types of glaucoma in rural West Bengal. The West Bengal Glaucoma Study. *The British Journal of Ophthalmology*. 2005;**89**(12):1559-1564
- [2] Song X, Song K, Chen Y. A computer-based diagnosis system for early glaucoma screening. In: Proc. IEEE Engineering in Medicine and Biology 27th Annual Conf. 2005. pp. 6608-6611
- [3] Eye Anatomy. Available from <http://www.optos.com/en-US/Patients/Healthy-sight/Eye-anatomy/> [Accessed: 15 December 2016]
- [4] Guyton AC, Hall JE. *Textbook of Medical Physiology*. 9th ed. Elsevier Saunders; 1996
- [5] Nath MK, Dandapat S. Techniques of glaucoma detection from color fundus images: A review. *International Journal of Image, Graphics and Signal Processing*. 2012;**4**:44-51
- [6] Mishra M, Nath MK, Nirmala SR, Dandapat S. Image processing techniques for Glaucoma detection. *Communications in Computer and Information Science: Advances in Computing and Communications*: Springer. 2011;**192**:365-373
- [7] Jonas JD, Nguyen XN, Naumann GOH. Parapapillary retinal vessel diameter in normal and glaucoma eyes: Morphometric data. *Investigative Ophthalmology & Visual Science*. 1989;**30**(7):1599-1603
- [8] Hall JK, Andrews AP, Walker R, Piltz-Seymour JR. Association of retinal vessel caliber and visual field defects in glaucoma. *American Journal of Ophthalmology*. 2001;**132**(6):857-859
- [9] Dua S, Acharya UR, Ng EYK. *Computational Analysis of the Human Eye with Applications*. World Scientific Press; 2011
- [10] Nayak J, Rajendra Acharya U, Bhat PS, Shetty N, Lim T-C, et al. Automated diagnosis of glaucoma using digital fundus images. *Journal of Medical Systems*. 2009;**33**:337-346. DOI: 10.1007/s10916-008-9195-z
- [11] Vijapur N, Chitins S, Kunte RSR. Improved efficiency of glaucoma detection by using wavelet filters, prediction and segmentation method. *International Journal of Electronics, Electrical and Computational System*. 2014;**3**(8):1-13
- [12] Uhm KB, Lee DY, Kim JT, Hong C. Peripapillary atrophy in normal and primary open-angle glaucoma. *Korean Journal of Ophthalmology*. 1998:37-50
- [13] Budai A, Odstrcilik J. High-Resolution Fundus (HRF) Image Database. Available from: <https://www5.cs.fau.de/research/data/fundus-images/>
- [14] Odstrcilik J, Kolar R, Budai A, Hornegger J, Jan J, Gazarek J, et al. Retinal vessel segmentation by improved matched filtering: Evaluation on a new high-resolution fundus image database. *IET Image Processing*. 2013;**7**(4):373-383. DOI: 10.1049/iet-ipr.2012.0455
- [15] Lowell J, Hunter A, Steel D, Basu A, Ryder R, Fletcher E, et al. Optic nerve head segmentation. *IEEE Transactions on Medical Imaging*. 2004;**23**(2):256-264
- [16] Real Statistics Using Excel: Correlation: Basic Concepts, Available from: <http://www.real-statistics.com/correlation/> [Accessed: 22 February 2015]

- [17] Nataraj A Vijapur, R. SR Kunte. Glaucoma detection by using Pearson-R correlation filter. In: Proc. 4th IEEE International Conference on Communication and Signal Processing (ICCSP'15). 2015; 1194-1198. DOI: 10.1109/ICCSP.2015.7322695
- [18] Vijapur NA, Kunte RSR. Sensitized glaucoma detection using a unique template based correlation filter and undecimated isotropic wavelet transform. *Journal of Medical and Biological Engineering*. 2017;37:365. DOI: 10.1007/s40846-017-0234-4
- [19] Nyúl LG. Retinal image analysis for automated glaucoma risk evaluation. In: Liu J, Doi K, Fenster A, Chan SC, editors. *Medical Imaging, Parallel Processing of Images, and Optimization Techniques*. Vol. 7497. 2009. pp. 74971C-1-74971C-9. DOI: 10.1117/12.851179
- [20] Xu Y, Xu D, Lin S, Liu J, Cheng J, Cheung CY, et al. Sliding window and regression based cup detection in digital fundus images for glaucoma diagnosis. *LNCS*. 2011;6893:1-8
- [21] Patton N, Aslam TM, MacGillivray T, Deary IJ, Dhillon B, Eikelboom RH, et al. Retinal image analysis: concepts, applications and potential. *Progress in Retinal and Eye Research*. 2005:99-127
- [22] Lee SB, Hong KBUC. Retinal vessel diameter In normal and primary open angle glaucoma. *Korean Journal of Ophthalmology*. 1998;12:51-59
- [23] Starck J-L, Fadili J, Murtagh F. The undecimated wavelet decomposition and its reconstruction. *IEEE Transactions on Image Processing*. 2007;16(2):297-309
- [24] Dua S, Acharya UR, Chowriappa P, Sree SV. Wavelet-based energy features for glaucomatous image classification. *IEEE Transactions on Information Technology in Biomedicine*. 2012;16:80-87. DOI: 10.1109/TITB.2011.2176540.
- [25] Levenberg K. A method for the solution of certain non-linear problems in least squares. *Quarterly of Applied Mathematics*. 1944;2:164-168
- [26] Auer P, Burgsteiner H, Maass W. A learning rule for very simple universal approximators consisting of a single layer of perceptrons. *Neural Networks*. 2008;21(5):786-795